

Michael R. Hill<sup>1</sup> and Tina L. Panontin<sup>2</sup>

## EFFECT OF RESIDUAL STRESS ON BRITTLE FRACTURE TESTING

---

**REFERENCE:** Hill, M. R., and Panontin, T. L., “Effect of Residual Stress on Brittle Fracture Testing,” *Fatigue and Fracture Mechanics: 29<sup>th</sup> Volume, ASTM STP 1332*, T.L. Panontin and S.D. Sheppard, Eds., American Society for Testing and Materials, 1998.

**ABSTRACT:** Residual stress present in coupons used for fracture testing will influence the experimental determination of fracture toughness. Triaxial residual stress (e.g., due to welding) can alter both the driving force for fracture and the crack-tip constraint at a specified load, so that the apparent toughness of a coupon depends on the residual stress present. In this paper, we employ a micromechanical failure theory (the RKR model) to predict brittle fracture loads for three-point bend samples with and without triaxial residual stress. Finite element modeling is used in the study to introduce an idealized welding residual stress field, to simulate the crushing of the coupon by circular platens (referred to as homogenization or local compression), and to simulate three-point bend testing. Results show that the residual stress markedly changes load at fracture, which would be used to compute apparent fracture toughness. Furthermore, the method of superposition commonly used is not able to accurately predict this effect.

**KEYWORDS:** residual stress, weld fracture, fracture toughness testing, superposition, micromechanical models, brittle fracture, homogenization

---

### Introduction

Fracture of welded connections often occurs at loads drastically different from loads which would cause fracture in the same structure without a weld. There can be several reasons for this phenomenon and the most widely accepted influences are defects from the welding process, material variations induced by the weld thermal cycle, and residual stresses. In this paper, we examine computationally the influence of residual stress on weld fracture and focus on demonstrating how residual stress can influence the determination of fracture toughness in weld metals.

---

<sup>1</sup> Assistant Professor, Mechanical and Aeronautical Engineering Department, University of California, Davis, CA 95616-5294, mrhill@ucdavis.edu

<sup>2</sup> Group Leader, Materials and Failure Analysis, Systems Engineering Division, NASA-Ames Research Center, MS 213-4, Moffett Field, CA 94035-1000, tpanontin@mail.arc.nasa.gov

A previous computational study conducted by the authors [1] indicated that residual stress can cause fracture to occur at applied loads well below those predicted using the assumption of  $J$ -integral controlled fracture. The study demonstrated that triaxial residual stresses typical of welding can alter constraint at the crack-tip at the same time that they alter the crack driving force. In the structure examined, a cylindrical pressure vessel with a 360° part-through circumferential crack, residual stresses doubled the crack-driving force near brittle fracture loads and at the same time drastically increased the  $Q$ -value from -0.7 without residual stress to -0.1 at the same level of  $J$ .

The focus of this paper is to determine whether residual stresses can induce similar constraint changes in three-point bend fracture specimens typically used for fracture toughness testing. Of concern is the determination of the true toughness for brittle fracture of weld metal when residual stresses are present. Several different specimen conditions are considered, namely without residual stress, with residual stress, and with residual stress and *homogenization*, a process used to modify existing residual stress. Results of the study indicate that residual stresses in fracture specimens affect the crack driving force at a given load, and that they induce toughness changes at brittle fracture loads due to constraint increases. The homogenization process itself is shown to increase constraint. The implications of these results for the determination of weld fracture toughness in the presence of residual stresses are discussed.

## Residual Stress Distribution

Residual stresses arise from most mechanical or thermal operations performed in processing engineering materials. For welding, residual stresses are caused by the thermal cycle that occurs when hot weld metal is laid on much cooler base metal or previous weld passes. Subsequent cooling causes thermal, plastic, and transformation strains to set up in the material, and these strains give rise to residual stress. Residual stress is in fact entirely determined by the geometry of the structure and the distribution of *eigenstrain*, a combination of all the non-elastic, incompatible strains set up during the welding cycle [2]. The eigenstrain field induced by a particular welding process must be found either experimentally [3] or using non-linear thermo-elasto-plastic analysis (TEPA) [4][5]. However, once the eigenstrain field is known, residual stress at every point within a welded structure can be found from a *linear elastic* analysis using the theory of elasticity or an approximation such as the finite element method (FEM) [6]. Elastic theory can be used to find residual stress in the structure because residual stresses are at equilibrium and do not cause active yielding; therefore, a properly defined eigenstrain field must give rise to stresses which satisfy a specified yielding condition (e.g., vonMises equivalent stress less than yield strength) in an elastic body. However, once a defect is introduced into a structure, elastic-plastic analysis may need to be performed to account for yielding of material at the crack-tip.

Here we consider a structure in which the residual stresses predate the flaw and where the unflawed residual stress state is given by an arbitrary, but known, eigenstrain field. Finding the elastic-plastic stress distribution for the flawed geometry is accomplished by imposing the eigenstrain field in a finite element model with the crack faces restrained and finding the equilibrium (residual) stress state. At this, and subsequent, steps in the analysis the material is modeled as elastic-plastic. However, in this first step,

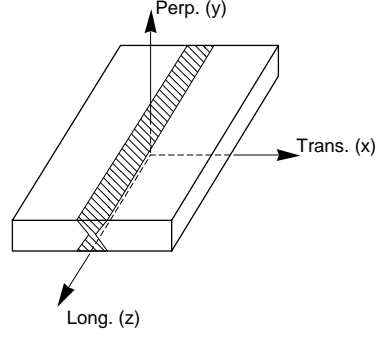


**Figure 1** – Coordinate directions with respect to a butt-welded plate

no plastic deformation will occur as we require the eigenstrain field to satisfy the yielding condition when imposed in an elastic body. Following the initial step, the crack is gradually opened by releasing crack-face tractions sequentially to achieve a desired crack length. During the opening process, plastic deformation may occur and if it does, a plastic zone caused by the residual stress field will develop.

In this paper we make use of an assumed eigenstrain distribution. This distribution gives rise to residual stresses that are typical of a continuously welded, double-sided joint in mild steel plate [7]. The eigenstrain field used in this paper is the same as that used to induce residual stress in the previous study of a cracked pressure vessel [1] and is similar to one used in another context to simulate multipass weld residual stress [6]. Relative to the coordinate directions shown in Figure 1, this eigenstrain distribution is given by

$$\{\varepsilon^*_{xx}, \varepsilon^*_{yy}, \varepsilon^*_{zz}\} = \{-0.004, -0.004, -0.001\} * f(x/t) * g(y/t)$$

$$\varepsilon^*_{xy} = \varepsilon^*_{yz} = \varepsilon^*_{xz} = 0 \quad (1)$$

where, for  $|x/t| \leq 1.0$

$$f(x/t) = 0.5[1 + \cos(\pi(x/t))]$$

$$g(y/t) = 0.5[1 + \cos(2\pi(y/t))]$$

and, for  $|x/t| > 1.0$

$$f(x/t) = g(y/t) = 0.$$

All coordinates have been normalized in Equation (1) by the plate thickness,  $t$ . The function  $f(x/t)*g(y/t)$  is plotted in Figure 2 to help in visualizing the eigenstrain field. Note that the continuous welding assumption means that the eigenstrain distribution left in the wake of the weld is *independent* of position along the weld (coordinate  $z$ ) [3]. Accordingly, the eigenstrain function assumed in this study depends only on the transverse and perpendicular welding directions,  $x$  and  $y$ .

The use of an eigenstrain distribution offers several advantages for further analysis. First, the residual stress present in a welded structure can be determined by imposing the eigenstrain distribution in a finite element model of the geometry. Although that analysis is complicated by the spatial variation of each eigenstrain component, a general-purpose finite element program can be used to produce the residual stress estimates. Second, the removal of fracture samples that include some portion of the weld region from the larger structure can be simulated by simply imposing the eigenstrain distribution on the removed sample geometry (i.e., the cutting process is assumed to produce only *elastic* deformations). This means the actual removal process does not need to be modeled in

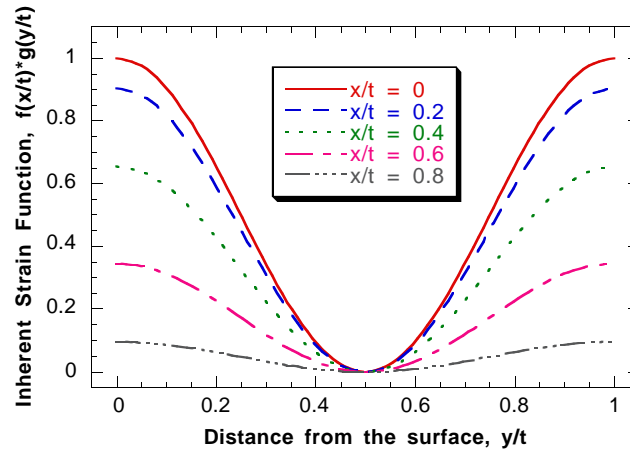


**Figure 2** – Function giving the spatial variation of eigenstrain assumed to be typical of the field in a double-sided butt-welded plate

detail, as long as the elastic-deformation assumption is not violated. In a flawed sample, plastic deformation in the vicinity of the crack-tip can be handled by gradually opening the crack, as described above. Using this approach, the release of stress which accompanies sample removal from the larger structure is accounted for. Therefore, making use of a known (or, in the present work, assumed) eigenstrain distribution admits the availability of a welded structure and fracture specimens removed from that structure in which the residual stresses are easily determined. Further, the full-field triaxial residual stress state is known at every point within any sample removed from the weld region.

Variation of residual stress along the crack-front of specimens removed from welded joints causes problems when attempting to pre-crack samples in actual testing. A proposed Annex to ASTM Test Method for Crack-Tip Opening Displacement (CTOD) Fracture Toughness Measurement (E1290) espouses homogenization (also called local compression) as a means to mitigate the effect of residual stress variation on pre-crack straightness<sup>1</sup>. Homogenization consists of compressing a specimen in the through-thickness direction near the crack-tip, as shown in Figure 3(a). Displacements applied to the specimen by the circular platens must produce sufficient plasticity to overwhelm the effect of the variation of weld residual stresses (a total plastic reduction in specimen thickness of  $0.8\% \pm 0.2\%$  is suggested in the proposed Annex). In this study, we investigate the influence of homogenization on fracture testing by simulating the process and the subsequent fracture testing of homogenized samples.

## Material and Specimen Geometry

The material properties used in this investigation are those of A516 Gr70, a high hardening, ferritic, pressure vessel steel, which is typically used for welded vessels operating at moderate to low temperatures. In the normalized condition, this material has a

<sup>1</sup> Draft Weld Fracture Test Standard (Proposed Annex to ASTM E1280), draft dated April, 1996.

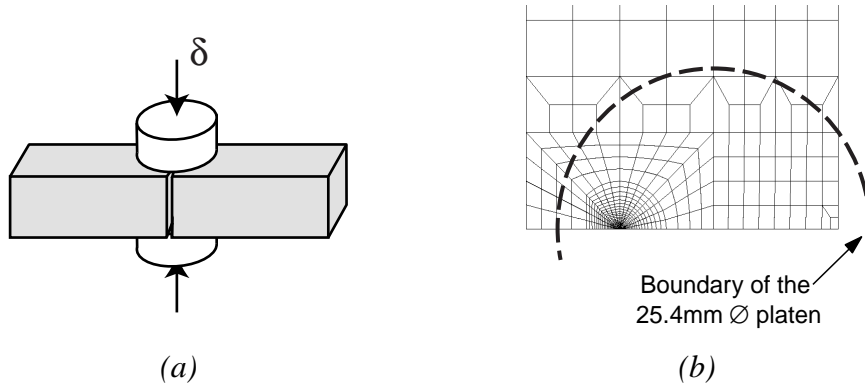


**Figure 3** – (a) Homogenization process described in proposed Annex to ASTM E1290  
 (b) Region where displacements are applied to simulate homogenization

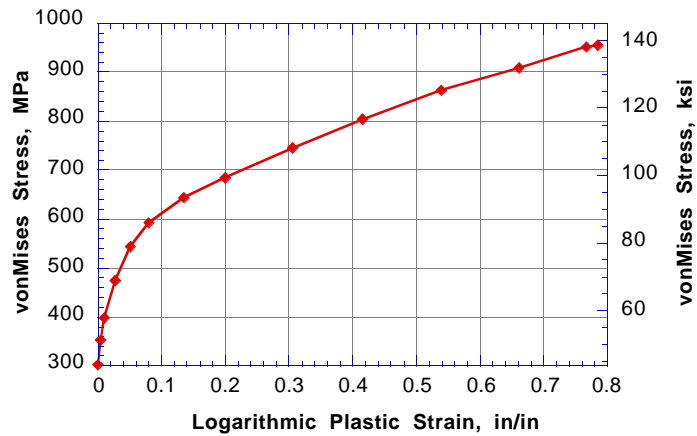


**Figure 4** – True stress vs. logarithmic plastic strain measured for A516-70 [1]

yield strength,  $\sigma_o$ , of 303 MPa (44 ksi) and an average grain size of 0.05 mm (0.002 in). The stress-strain properties measured for 25.4 mm (1.0 in) thick plate are shown in Figure 4 [1]. These properties are similar to those obtained in welds made in A516-70 with E5018 rod.

The geometry of the three-point bend (or, SE(B)) specimens studied is shown in Figure 5. This specimen meets ASTM Fracture Toughness Test Requirements (E399, E813, etc.) except for the shorter crack size of  $a/W = 0.3$ . In the authors' earlier study of a flawed pressure vessel [1], this size was selected to correspond with realistic flaws encountered in welded pressure systems. The same flaw size was used in this study for compatibility with the earlier work. The specimens studied are located in the weld in two different orientations, T-S and T-L, as shown in Figure 6. As described above, the residual stresses present in each specimen can be found using FEM and the eigenstrain distribution given in Equation (1). The only distinction between the two specimens is the orientation of the weld within the sample; no effort is made to model material anisotropy.

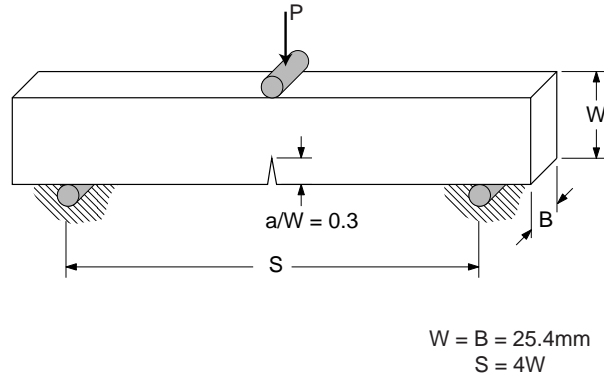


**Figure 5** – SE(B) specimen geometry with applied loading indicated

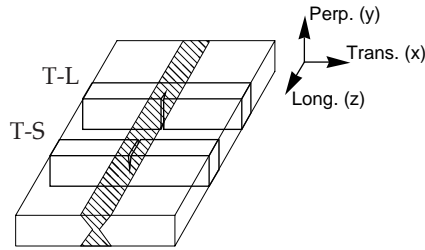


**Figure 6** – Two different orientations of transverse fracture specimens studied

The different orientation with respect to the welding direction greatly changes the characteristics of the residual stress field in each specimen. In the T-S sample, the eigenstrain field is uniform along the longitudinally-oriented crack-front. This imposes residual stresses which are mostly uniform along the crack-front, except near the surfaces of the specimen. In the T-L specimen, the eigenstrain field varies widely along the crack-front, which lies along the perpendicular welding direction. This variation from maximum to minimum to maximum is shown in Figure 2. Accordingly, the crack-tip stresses will vary widely with position along the crack-front which would cause problems in fatigue pre-cracking. This variation also impacts the scheme used to predict fracture in the presence of residual and applied stresses.

### **Micromechanical Model of Brittle Fracture**

Prediction of brittle fracture is often performed by assuming that global fracture parameters such as the  $J$ -integral,  $J$ , or the Mode-I stress intensity factor,  $K_I$ , control the fracture event. The usual method in the presence of a known residual stress field is to use superposition. In linear elastic fracture mechanics this is accomplished by finding the stress intensity factor caused by residual stress and adding it to that caused by applied loading. The situation is more difficult for the elastic-plastic case, but two approaches have been used previously. One can either include residual stress in a non-linear finite element computation which can provide a  $J$ -integral estimate, or include residual stress as a

secondary stress, accounting for its contribution to only the elastic part of  $J$  [8]. The second approach is more approximate as it ignores the relaxation of residual stress which accompanies increasing applied loading.

Which ever method is used to include the residual stresses, an approach to fracture prediction which assumes  $J$  or  $K_I$  controlled fracture ignores the influence of *constraint* which has been shown to cause large changes in brittle fracture toughness [9]. Constraint changes affect the magnitude of the crack-tip stresses which is not reflected in global fracture parameters. It is generally accepted that different levels of constraint can exist in structures due to differences in geometry (e.g., thick versus thin) or applied loading (e.g, tension versus bending). However, it is also possible that constraint changes can occur due to the presence of different distributions of residual stress. Previously the authors have demonstrated this effect for residual stress in welded structures; as might be expected, the predicted influence was found to be much greater for brittle fracture than for ductile fracture in high toughness materials [1].

In the current study, it is hypothesized that residual stresses may alter the constraint conditions in fracture specimens, and hence, it is necessary to examine crack-tip stresses directly. The approach pursued here uses FEM to simulate applied loading for the fracture testing of three-point bend specimens which have been removed from a welded structure and loaded as shown in Figure 5. Data from the simulation provide the crack-tip stress state as a function of increasing applied load which can then be used within a micromechanical model to predict brittle fracture.

Unstable cleavage fracture in mild steels is generally associated with microcracks, formed within brittle grain boundary particles by twinning or slip dislocation pile-ups, that grow into the ferrite matrix under the action of tensile stress. In the micromechanical model proposed by Rice, Knott, and Ritchie (RKR model) [10] for slip-initiated, transgranular cleavage fracture, initiation is said to occur when the opening stress,  $\sigma_{yy}$ , at the crack-tip exceeds the fracture stress,  $\sigma_f^*$ , over a critical distance,  $l^*$ , which is on the order of the grain size of the steel. This criterion is shown schematically in Figure 7.

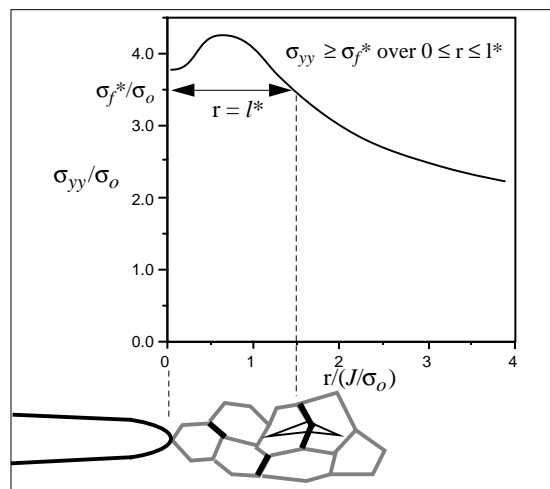


**Figure 7** – Schematic representation of the micromechanical brittle fracture initiation model (after [11])

Accordingly, predictions of fracture initiation are made by examining the distribution of opening stress (as predicted by the finite element analysis) with distance ahead of the crack-tip as a function of load. The load at which crack initiation occurs is said to be reached when the opening stress exceeds a critical value over the critical length,  $l^*$ . The location of crack initiation, e.g., whether at  $0^\circ$  or  $45^\circ$  from the crack plane, is predicted to be where the initiation criterion is first satisfied. Once the fracture initiation load is identified using this procedure, the global fracture parameters (e.g.,  $J$ -integral) associated with that load are obtained from the finite element analyses.

Previous studies concerning cleavage fracture indicate that the critical fracture stress ranges from 3 to 4 times the yield strength of the material, and that it is relatively independent of temperature and strain rate [10]. Estimates of the characteristic length or distance in mild steels range from 2 to 5 grain diameters [10]. For the purpose of demonstrating the qualitative effect of residual stresses on brittle fracture, it is not necessary to know precisely the values of the critical stress and distance as long as consistent values are used. In this study of A516-70 steel, a critical value of the opening stress is taken to be 3.5 times the yield strength and a critical distance of 0.15 mm (0.006 in), or about 3 ferritic grain diameters, is assumed. Hence, the criterion for brittle fracture may be written as

$$\frac{\sigma_{yy}}{\sigma_o} > 3.5 \text{ over } 0 \leq r \leq 0.15 \text{ mm} \quad (2)$$

### Constraint Analyses

The change in constraint conditions due to the influence of the residual stress field is quantified using  $J$ - $Q$  theory. The theory uses the approximate two-parameter description of the crack-tip stress-strain fields developed from asymptotic analyses and finite element simulations performed by O'Dowd and Shih [12][13]. These stress fields are applicable to small and large scale yielding conditions and can be written as

$$\sigma_{ij} = \sigma_o f_{ij}(r/(J/\sigma_o), \theta, Q) \quad (3)$$

where  $r$  and  $\theta$  are polar coordinates centered at the crack-tip and the parameter  $Q$  is dimensionless. As a measure of how much  $\sigma_{ij}$  differs from the adopted small scale yielding (SSY) reference solution at the same applied  $J$ , the parameter  $Q$  has been shown to characterize the magnitude of the hydrostatic stress over the forward sector ahead of the crack-tip (i.e.,  $\theta < \pi/2$  and  $1 < r/(J/\sigma_o) < 5$  to a good approximation.  $Q$  is formally defined as

$$Q = [\sigma_{\theta\theta} - \sigma_{\theta\theta}|_{\text{SSY}}]/\sigma_o \text{ at } \theta = 0, r/(J/\sigma_o) = 2 \quad (4)$$

and is obtained from stresses predicted straight ahead of the crack-tip by finite element analyses of both finite and infinite size (SSY) crack geometries. By definition,  $Q = 0$  in all crack geometries under small scale yielding conditions. However, as deformation levels increase in finite size specimens, the hydrostatic stresses at the crack-tip are relieved and fall below those that exist in an infinite cracked body at the same  $J$ -value. This produces a negative  $Q$ -value, which denotes a loss in constraint. A positive  $Q$ -value indicates that high constraint exists for a particular geometry and loading condition [14].

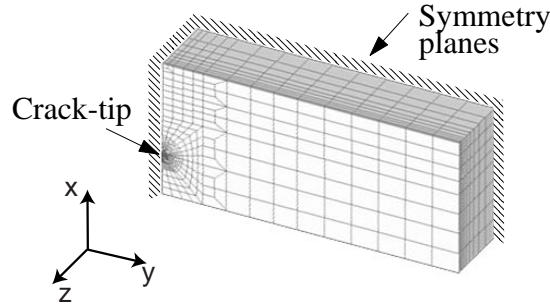


**Figure 8** – FEM mesh used to simulate fracture toughness testing and coordinate system used in discussing fracture results

In this study, we choose to compute  $Q$  further away from the crack-tip than the standard distance of  $r/(J/\sigma_o) = 2$  because, in the analysis of brittle fracture, the stress state at small values of  $J$  is required, calling for stress estimates at extremely small distances ahead of the crack-tip,  $r$ . Even with a crack-tip element size of 0.0076 mm (0.0003 inch), use of  $r/(J/\sigma_o) = 4$  is required to obtain accurate estimates of  $Q$  at the  $J$ -levels where brittle fracture initiation is predicted using the micromechanical theory.

### Simulation Procedures

A finite element mesh of the SE(B) geometry was generated using the PATRAN3 modeling package [15] as shown in Figure 8. Also shown in the figure are the coordinates used in the fracture analyses. We make a change in coordinates relative to those used in discussing welding (Figure 1), so that all specimens can be easily compared (e.g., opening stress in all specimens is referred to as  $\sigma_{yy}$ ). Elastic-plastic finite element analyses were conducted utilizing ABAQUS 5.5 [16]. The finite element solutions employ nonlinear, large deformation material and geometry relations. Linear eight-noded hexahedral elements are used, with selective reduced integration to eliminate artificial locking under incompressible deformation conditions. Plasticity is modeled using incremental theory with a vonMises yield surface, associative flow rule, and isotropic hardening. Flow properties are described by a piece-wise linear fit to true stress, logarithmic strain data gathered for A516-Gr70 plate [1], adjusted for necking effects by the Bridgman correction [17], and shown in Figure 4. Differences between weld and plate material properties are not modeled. Also, the influence of residual stress on crack-front shape following fatigue pre-cracking has not been included as the model shown in Figure 8 contains a straight crack-front.

By exploiting symmetry conditions, including symmetry of the eigenstrain distribution, only one-fourth of the SE(B) geometry was modeled. The element size at the crack-tip is 0.0076 mm (0.0003 inch) and the crack-tip is modeled with a finite radius of 0.0051 mm (0.0002 inch) in anticipation of crack-tip blunting. The three-dimensional model has 10 layers through the thickness with a layer-thickness ratio of 10:1 between midplane and free-surface. Three-point bend loading is simulated by imposing applied displacements over a finite area near the symmetry plane. The most complicated simulation using this symmetric mesh, with roughly 8400 elements and 10000 nodes,

requires about 15000 seconds of run time on a Hewlett-Packard C-100 workstation to complete 21 load increments with an average of 3.5 iterations per increment. Small increments of load are taken to ensure that development of the crack-tip stress and strain history can be monitored.

At each load increment, the  $J$ -integral was calculated by the domain integral method implemented in ABAQUS 5.5. Hence, the reported  $J$  data include the additional driving force due to the residual stresses. A minimum of 25 crack-tip domain contours was used to insure evaluation on domains outside the blunted region. The validity of the finite element computation of the  $J$ -integral was verified for a similar residual stress field in an elastic single edge cracked plate ( $a/W = 0.30$ ) through comparison with an available weight function [18]. Results agreed within 3%.

The accuracy of the finite element predictions in the absence of residual stress was studied extensively. The effect of variation in plate flow properties was examined. Mesh refinement studies of the crack-tip region and initial crack-tip radius were performed to ensure convergence of the predicted crack-tip deformation and associated stress-strain fields. In addition, numerous experimental measurements of load-displacement and load-strain behaviors, and deformed shape, were made and compared to finite element predictions. The results of these convergence studies and experimental measurements are reported elsewhere [19][20].

Our goal in this paper is to demonstrate the effect of residual stress *and* homogenization on fracture toughness testing. Therefore, five different sample types have been simulated: a plain specimen with no residual stress, two T-S specimens, one with homogenization and one without, and likewise two T-L specimens.

As described above, residual stress distributions in the specimens were imposed using an eigenstrain distribution (i.e., that described by Equation (1)). Past methods have imposed residual stress using a temperature distribution and isotropic thermal expansion within the weld region [21]. For welding, the eigenstrain field is not necessarily isotropic and therefore isotropic thermal strain imposed through a simple temperature distribution cannot accurately represent the residual stress field. Our approach is to spatially distribute *anisotropic* thermal expansion properties within the specimen. At each point in the model the thermal expansion tensor is set equal to the value of the eigenstrain tensor at that point. The model is then loaded by applying a unit temperature increase, thereby imposing the eigenstrain field of interest. With the eigenstrain distributed, equilibrium is found using an FEM solver, and the complete triaxial residual stress state is found at every point within the body.

Homogenization of the SE(B) specimens is simulated by imposing applied displacements in the thickness direction in Figure 5 to -0.5% of the specimen thickness as shown schematically in Figure 3(a). The region of application of the homogenization displacements on the FEM mesh is shown in Figure 3(b). The displacements are applied incrementally to capture the history of the non-linear process, and then the applied displacements are released leaving the specimen in a state of altered residual stress. This process results in a plastic thickness reduction of 0.4% in the model (0.8% reduction when symmetry is considered). In actual testing, homogenization would be followed by fatigue pre-cracking prior to loading to fracture. To simulate the pre-cracking process, crack-face nodes within  $0.05W$  behind the crack-tip in the SE(B) mesh are restrained during the homogenization process and then released after homogenization loads are removed. This

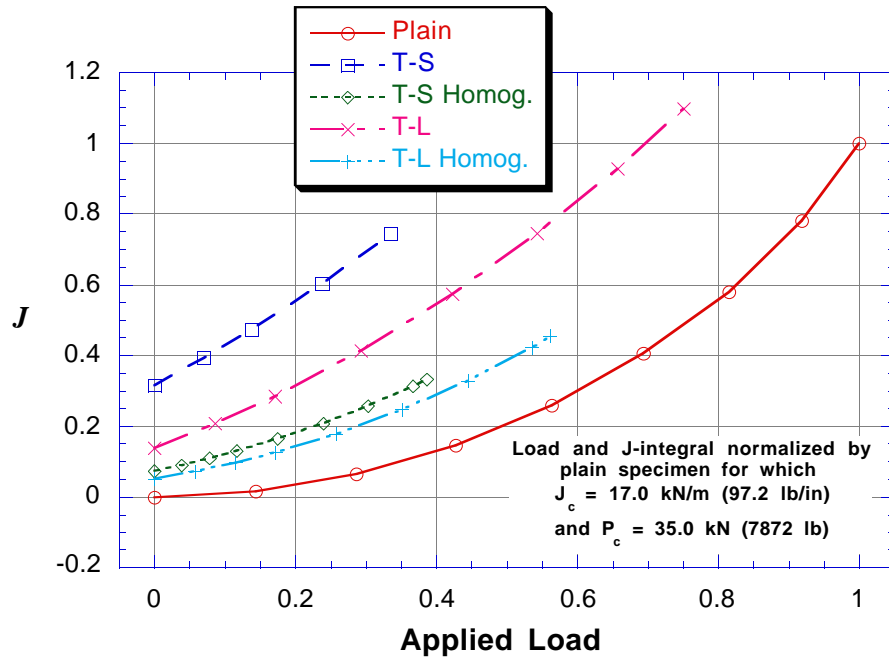


**Figure 9** – *J*-integral as a function of applied load computed using the domain integral method employed by ABAQUS 5.5 (results normalized by the residual-stress-free case)

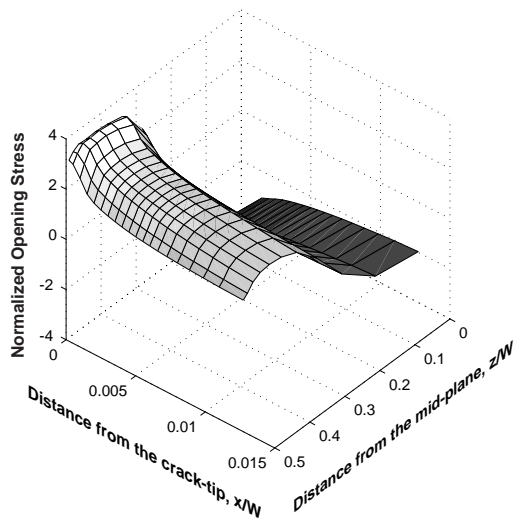
strategy leaves a plastic zone due only to residual stress remaining after homogenization; however, no attempt is made to account for the cyclic plasticity which would accompany fatigue pre-cracking. Simulation of the homogenized test specimen, then, consists of five steps: 1) find residual stress (equilibrium) in the presence of the eigenstrain field, 2) apply homogenization displacements, 3) release homogenization displacements, 4) release crack-face tractions to simulate crack extension, 5) apply three-point bend loads to fracture.

## Results

### *Finite Element Simulations*

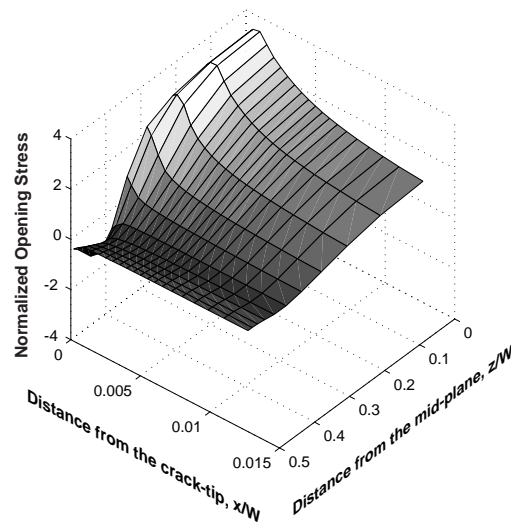
*J*-integral versus load data are plotted in Figure 9 for each of the five load cases described above. These data show that the residual stress state changes the crack-driving force, *J*, at a given load. Both the specimen orientation and the process of homogenization change the crack driving force at zero applied load, the *J*-integral due to residual stress alone. In fact, the entire crack-tip stress state prior to loading is altered by homogenization. For the T-L orientation, not only is the crack-tip opening stress affected, as shown in Figure 10, but also crack-tip triaxiality, the ratio of hydrostatic stress to vonMises equivalent stress ( $\bar{\sigma}/\sigma'$ ), as shown in Figure 11.

For every specimen condition but one, the *J*-integral and opening stress was a maximum at the mid-thickness of the bend specimen. However, the *J*-integral for the non-homogenized T-L specimen is maximized at an intermediate point along the



T-L, residual stress only

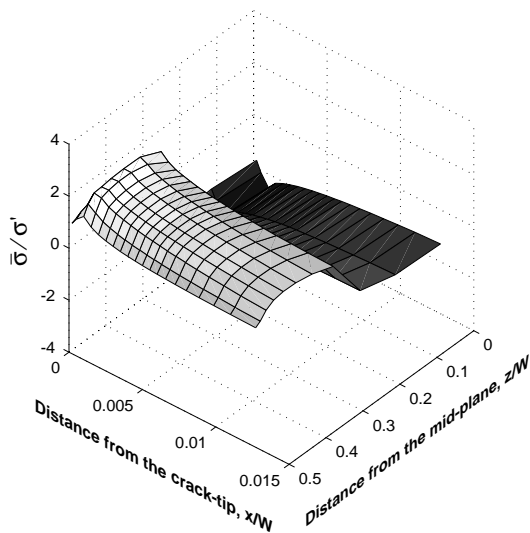
(a)



T-L, homogenized

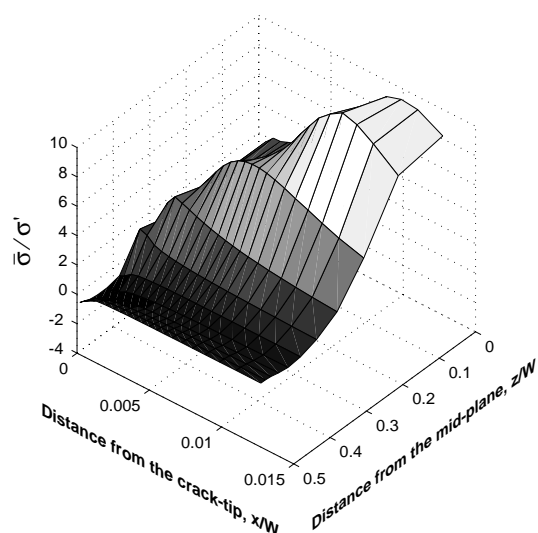
(b)

**Figure 10** – Crack-tip distribution of opening stress for the T-L specimen before, (a), and after, (b), homogenization (stresses normalized by  $\sigma_o$ ).



T-L, residual stress only

(a)



T-L, homogenized

(b)

**Figure 11** – Crack-tip distribution of triaxiality for the T-L specimen before, (a), and after, (b), homogenization (note the difference in triaxiality scale in the two plots).

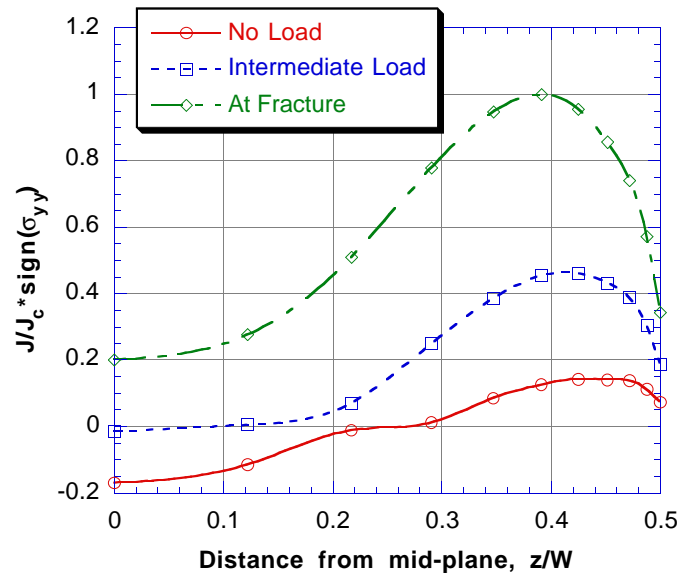


**Figure 12** – Variation of  $J$  with position along the crack-front for the T-L specimen.  $J$  has been multiplied by the algebraic sign of the opening stress along the crack-front.

crack-front, as would be expected given the variation in residual opening stress along the crack-front shown in Figure 10(a). The distribution of  $J$  along the crack-front at three different load levels is shown in Figure 12. Although the peak in the  $J$  vs.  $z$  curve shifts toward the mid-thickness with increasing load, all  $J$ -integral results and crack-tip stresses used in the failure model for the T-L specimen are reported on the plane on which  $J$  is a maximum at predicted fracture (about 10% into the thickness, as shown in Figure 12).

### *Micromechanical Fracture Predictions*

In Figure 9 the final point on each  $J$ -integral curve is the point of fracture predicted using the RKR model. Load required for fracture is shown to vary widely with specimen orientation and with homogenization. Summary plots comparing predicted load and  $J$ -integral at fracture are shown in Figure 13 for the four residual stress specimens. Results in the figure are normalized by the fracture conditions of the plain specimen. The results of a superposition analysis, also shown in the figure, will be described below. The RKR model predictions show that residual stress has a significant impact on fracture load, especially for the T-S specimen. Not only is there an impact on fracture load, but also on the  $J$ -integral at fracture. These results further demonstrate that the process of homogenization, presumably used only to obtain a straight fatigue pre-crack, has an influence on the fracture conditions. While homogenization increases the fracture load by 16% for the T-S specimen, it decreases it by 25% for the T-L specimen, relative to the corresponding specimen without homogenization. However, this seemingly disparate influence on fracture load is accompanied by a shift in  $J$ -integral at fracture that is consistent; the values predicted for  $J_c$  decrease by 55% for the T-S specimen and 59% for

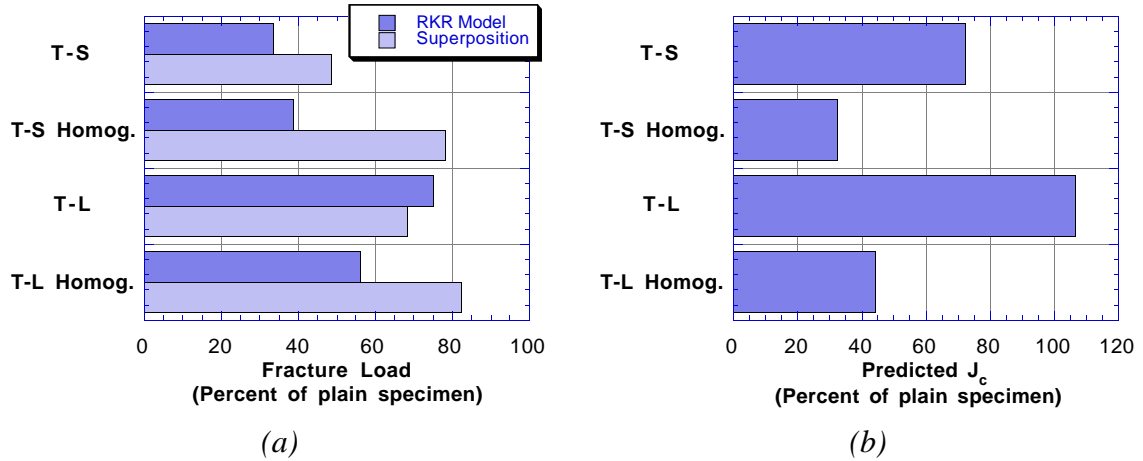


**Figure 13** – Comparison of predicted global parameters at fracture for the residual stress conditions examined: (a) Load and (b)  $J$ -integral.

the T-L specimen, relative to the corresponding specimen without homogenization. This significant drop in  $J_c$  is due to a change in constraint caused by homogenization as explained below.

#### Constraint Analyses

As might be suspected in view of the results shown in Figure 9 and Figure 11, the various specimen conditions create a wide variation of crack-tip stress field at a specified load. Crack-tip constraint is reflected quantitatively in the  $J$ - $Q$  trajectories for each specimen shown in Figure 14. Again, the final point on each curve represents the point of predicted fracture initiation. Here, we clearly see that welding residual stress impacts specimen constraint and also that the homogenization process greatly increases  $Q$ . The plain specimen starts with  $Q$  near zero and loses constraint (i.e.,  $Q$  decreases) with increasing load due to increasing plasticity. The T-S specimen starts with a positive value of  $Q$ , and this value decreases more slowly than was the case for the plain specimen. This behavior demonstrates that higher initial constraint ( $Q$ ) present in the T-S sample suppresses plastic flow relative to the behavior of the plain specimen as expected. On the other hand, the T-L specimen has low initial constraint which gives way to higher constraint with increasing load. This interesting behavior is possibly due to the variation of residual stress and  $J$ -integral through the specimen thickness. For both the T-S and T-L specimens, we find that the homogenized specimens have a much larger  $Q$ -value at the same  $J$  than the specimen without homogenization. Further, the trend in the final point on each  $J$ - $Q$  trajectory reflects a decrease in  $J_c$  with increasing constraint which is the expected influence of constraint on fracture.

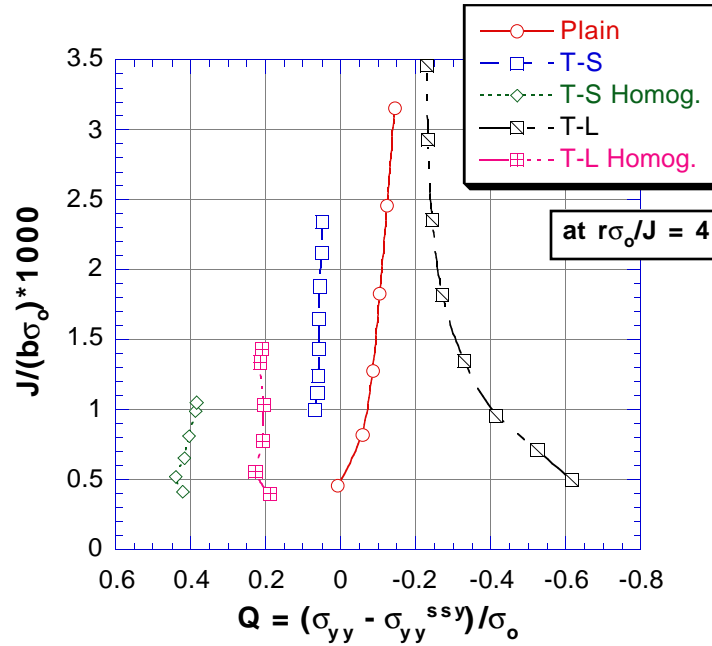


**Figure 14** –  $J$ - $Q$  trajectories for each of the five specimen types examined. The final point on each curve reflects predicted fracture.

## Discussion

### Comparison of Micromechanical and Conventional Superposition Approaches

The combination of results shown in Figure 9 and Figure 14 shows that weld residual stress and homogenization impact the crack-driving force and the constraint conditions at the crack-tip. If residual stresses are known, a common approach is to include the contribution of residual stress by considering its influence on the crack driving force and assume  $J$ -controlled (or,  $K$ -controlled) fracture behavior. For each specimen described above, we have computed the amount of applied load required to reach the critical  $J$ -integral estimated for the plain specimen,  $J_c^{Plain}$ . To do so, we assume the load- $J$  relation for a plain specimen and apply residual stresses to the elastic part of the  $J$ -integral as recommended in [8]. To obtain the elastic and plastic parts of  $J$ , we use the load- $J$  relations in ASTM Standard Test Method for  $J_{IC}$ , A Measure of Fracture Toughness (ASTM E813). In fact, the behavior of the plain specimen predicted with FEM and shown in Figure 9 is within 5% of the results of using ASTM E813. The  $J$ -integral due to residual stress in each specimen is obtained from the finite element results at zero applied load, and the total  $J$  is given by

$$J(P) = \{ \sqrt{J_{el}(P)} + \sqrt{J_{RS}} \}^2 + J_{pl}(P) \quad (5)$$

where,

$J(P)$  =  $J$ -integral at load  $P$ , including residual stress

$J_{el}(P)$  = elastic part of the  $J$ -integral, computed from relations in ASTM E813

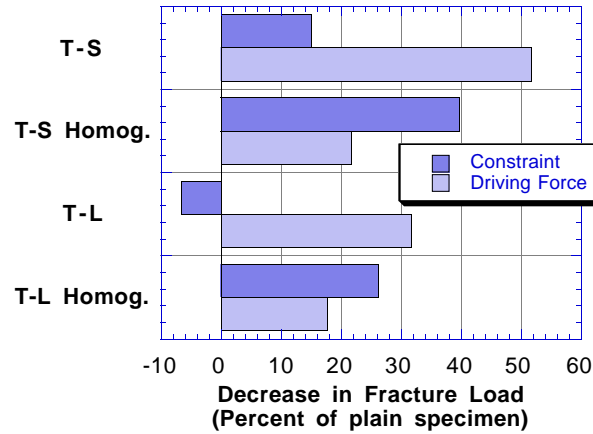


**Figure 15** – Decrease in fracture load due to driving force and to constraint derived from data given in Figure 13(a). The total load decrease predicted by the RKR model is the sum of the two values plotted for each specimen.

$J_{pl}(P)$  = plastic part of the  $J$ -integral, computed from relations in ASTM E813 and plain specimen displacement results

$J_{RS}$  =  $J$ -integral at no load from FEM computations

Results of iteration for the load at which  $J(P) = J_c^{Plain}$  are shown in Figure 13(a) together with the fracture loads predicted by the RKR theory.

Both sets of bars in Figure 13(a), taken together, allow separate comparison of the approximate influence of residual stress on driving force and on constraint. The difference between the fracture load predicted using superposition for each specimen and the fracture load of the plain specimen (100% in Figure 13(a)) gives the effect of driving force alteration alone. The difference between the RKR and the superposition predictions shows the effect of constraint change alone. Results of computing these differences are shown in Figure 15. For the as-welded samples the influence of residual stress on driving force is larger while for the homogenized samples the influence on constraint is larger. This trend is due both to the reduction in  $J$ -integral at zero load (Figure 9) and to the generation of a localized hydrostatic stress (Figure 11) caused by homogenization.

### *Influence of Homogenization*

The variation of opening stress and  $J$  along the crack-front of the T-L specimen would quite likely cause problems in producing straight fatigue pre-cracks, as has been observed by several authors working with similar welded specimens [22]. The proposed homogenization procedure produces an opening stress distribution which has a much smaller variation along the crack-front, especially near the mid-thickness of the specimen. This evidence supports the use of homogenization to obtain a straight pre-crack for fracture toughness tests.

Previous experiments [23] examined the effect of homogenization on transverse weld stresses in a T-L specimen with  $a/W = 0.5$ ,  $B/W = 0.5$ , and  $W = 50$  mm (1.96 in). These experimental measurements of residual stress before and after homogenization are

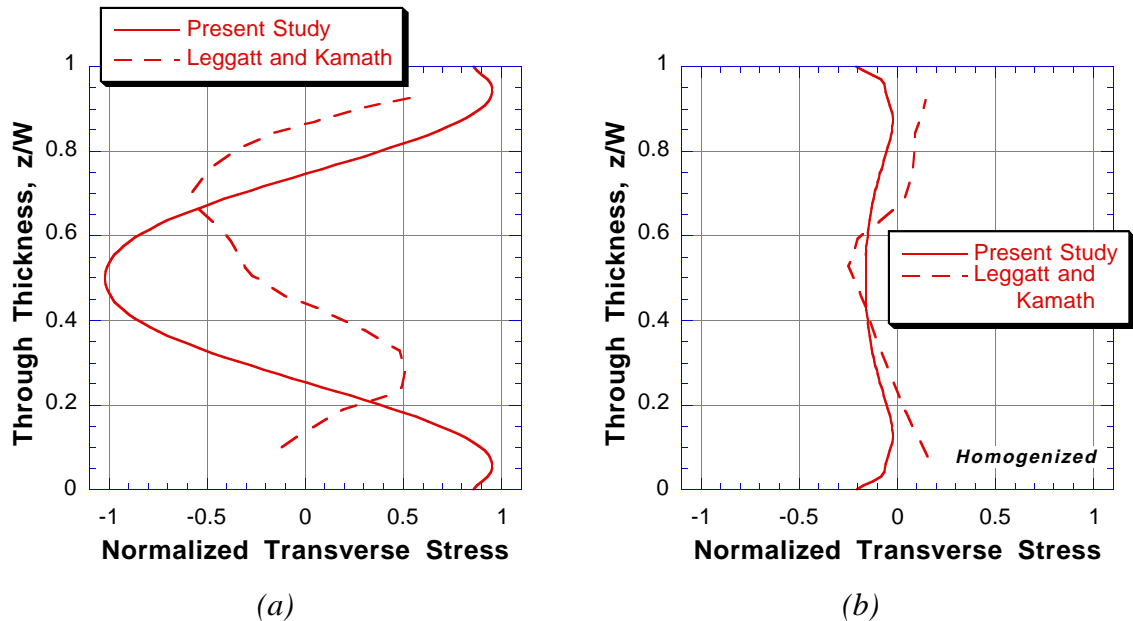


**Figure 16** – Residual stress before, (a), and after, (b), homogenization from the present work with experimental results from [23] (results for each study normalized by the respective base metal yield strength).

shown with the present simulation results in Figure 16. In the figure, the through-thickness distribution of residual stress is given on the crack-plane, at approximately the middle of the remaining ligament of the SE(B) specimens. Both the original and homogenized stress states are qualitatively in agreement. The large difference between Figure 16(a) and Figure 16(b) leads to the conclusion that homogenization has eliminated nearly all of the residual stress in the samples. However, that conclusion would be erroneous in view of the crack-tip stress fields shown in Figure 10(b) and Figure 11(b). Considering only the influence of the stresses remaining after homogenization, we see from Figure 9 that  $J$  at zero applied load in the homogenized specimens roughly corresponds to  $J$  at 30% of the fracture load in the plain specimen. So, although net-section stresses have been mostly relieved by homogenization, as shown in Figure 16, crack-tip stress remain significant. Nevertheless, the relatively uniform distribution of crack-tip opening stress which remains will likely yield a relatively straight fatigue pre-crack, as mentioned above.

Previous experimental work regarding the influence of homogenization on measured fracture toughness is also in agreement with the results described above. A review of this subject was provided by Towers and Dawes [22], where the effect of homogenization on normalized, low alloy steel plate and on stress-relieved and as-welded shielded metal arc (SMA) weld joints was examined. In the normalized plate, this study found a decrease in lower shelf critical CTOD ranging from 67% at -80C to 40% at -100C in 25mm (0.98 in) thick specimens. At higher temperatures (i.e., in the upper transition), a consistent effect of homogenization on critical CTOD could not be discerned. Similar trends were observed for the stress-relieved, single-vee SMA welds, in which a homogenization-induced decrease in critical stress intensity (i.e.,  $K_{Ic}$ ) of 28% at -100C

**Table 1: Effect of homogenization of T-L specimens on measured toughness**

<i>Source</i>	<i>Material</i>	<i>Specimen</i>	<i>Toughness Change</i>
[22]	TSR <sup>†</sup> single-vee weld	C(T)	-28% in $K_{IC}$
[22]	Normalized plate	Not stated	-40% to -67% in CTOD
[22]	Double-vee weld	Not stated	$\approx 0\%$ in $K_{IC}$
Present study	Idealized double-vee weld	SE(B)	-59% in $J^{Appl}$ ‡ -29% in $K_I^{Appl}$ ‡

† Thermally stress relieved (TSR)

‡  $J^{Appl}$  and  $K_I^{Appl}$  are computed using simulation load and displacement results in relations given in ASTM E813, thereby ignoring residual stress

was measured in compact tension testing. On the other hand, similar tests in 38mm thick double-vee SMA as-welded samples showed no significant influence of homogenization on measured toughness.

Results of the current study are compared with those presented in [22] in Table 1. There is a similar trend between the simulation and the experimental results for stress-relieved or unwelded samples. However, there appears to be some discrepancy between the simulation and experiments for the as-welded samples. One possible explanation may be a lack of crack-front straightness in the as-welded samples. Indeed, the fracture surface photos for as-welded specimens provided in [22] show a sharply varying crack-front profile. The simulations performed here do not include the influence of a non-straight crack-front.

In view of the experimental evidence and the computational work described here, it is clear that homogenization can provide needed benefits in terms of fatigue pre-cracking, but its influence on measured fracture toughness may present some difficulty. It has been suggested that the drop in toughness due to homogenization may be caused by strain-embrittlement [22] but the evidence here suggests that the drop is due mainly to residual stress. As mentioned above, residual stresses, whether from welding, from homogenization, or both, cause a change in both crack driving force and constraint at a given load. To capture these effects in a known residual stress field, it may be possible to use the type of modeling employed in this study to quantify the influence of homogenization on fracture behavior of test specimens.

#### *Quantification of Residual Stress and Homogenization Effects Using J-Q Theory*

Another approach to account for the influence of residual stress on driving force and constraint is to employ a two-parameter approach to fracture prediction. Taking the results at predicted fracture from Figure 14 we arrive at the fracture locus in  $J$ - $Q$  space shown in Figure 17. In the figure we have also included some results from the previous study on a flawed welded pipe [7] which also used the eigenstrain field given in Equation (1). The ability to combine the results for the various specimen conditions and geometries into a single locus is encouraging.

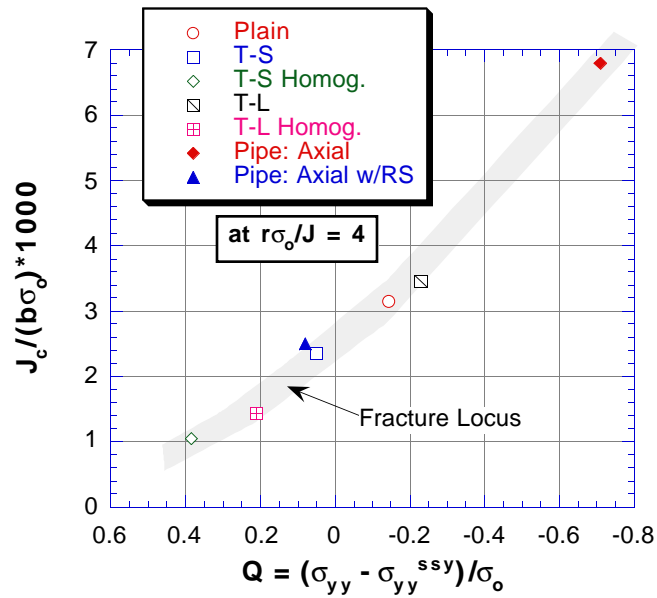


**Figure 17** – Point of predicted fracture in  $J$ - $Q$  space for each of the five specimen and for the axial load case of the pipe geometry studied in [1] with and without residual stress.

It may be possible to quantify the effect of homogenization using the observation that the process causes a  $Q$ -shift of about +0.4 and a  $J_{RS}$  of about 1.0 kN/m (5.8 lb/in) for both the T-S and T-L specimens. Taking a *two-parameter superposition* approach, one could superpose both the stress-intensity (or,  $J_{RS}$ ) and the  $Q$ -shift imposed by the homogenization process. In such an approach,  $J_{RS}$  would be factored in to the computation of measured toughness using Equation (5) and the  $Q$ -shift used to place the toughness measurement on a  $J$ - $Q$  fracture locus. Whether this approach is valid depends on several factors including: the consistency of the homogenization process in the presence of different residual stress fields and materials; the ability to determine the pre-existing residual stress field caused by welding; and, the ability of a linear superposition to approximate non-linear material behavior at the crack-tip.

#### *Prediction of Structural Behavior*

Taking a look at the larger problem of predicting structural behavior based on testing, we see that the SE(B) testing simulated here provides information over a range of  $Q$ . The structural simulation performed earlier [1] was conducted in a relatively low-constraint geometry dominated by tensile loading (Figure 17, “Pipe: Axial” case). In this structure, where the flaw was in the T-S orientation, the eigenstrain field given in Equation (1) gave rise to residual stresses which caused a very large shift in  $Q$  at fracture of +0.8 (from -0.7 without residual stress to +0.1). In the T-S test specimen, however, the change in constraint was only +0.2 in  $Q$  at fracture, or about 25% of the shift observed in the structure. This is likely due to the reduction of residual stress along the longitudinal weld direction (along the crack-front in the T-S specimen) which accompanies fracture

specimen removal from the larger structure. Where the longitudinal stresses were near yield-level in the structure, they are reduced to about 25% of yield in the removed sample. Nevertheless, we note that the  $J_c$  predicted for the pipe with residual stress and for the T-S SE(B) specimen are in close agreement; however, the agreement is likely serendipitous. This demonstrates an important influence of relatively small fracture specimen size when attempting to predict as-welded structural behavior with laboratory testing.

Prediction of the residual stress influence on weld fracture described here relies on detailed information on residual stresses. To be of value in elastic-plastic fracture simulation, residual stresses are needed at least where yielding is expected if not throughout the entire geometry of interest. The type of work reported here is possible only if either the eigenstrain field imposed by welding or the full-field, three-dimensional residual stress field is available for a structure of interest. Some progress has been made in experimental determination of eigenstrain due to welding [3] and continues to be made in welding simulation [4]. Without the availability of a detailed picture of weld residual stress, a simple eigenstrain distribution like that given in Equation (1) can at least provide reasonable insight into the qualitative influence of weld residual stresses on fracture behavior.

## Conclusions

We have described a number of computational simulations which demonstrate the influence welding residual stress and homogenization on the fracture behavior of three-point bend specimens. From this and a previous study, as well as a summary of available experimental results, the following conclusions can be drawn:

- Residual stress affects both the driving force for fracture and constraint conditions at the crack-tip. Together these effects decrease the fracture load for the specimens studied.
- A traditional driving-force superposition approach to fracture prediction in the presence of residual stresses is inadequate because it ignores the effect of residual stress induced constraint.
- A two-parameter approach to fracture prediction appears to hold promise for predicting the influence of residual stress on brittle fracture.
- The amount of constraint generated by an idealized weld eigenstrain field is far smaller in fracture specimens than in a structural geometry previously studied.
- Homogenization decreases the crack-driving force due to residual stress and increases crack-tip constraint.
- A homogenization-induced decrease in fracture load appears to be caused by the production of a triaxial residual stress field which increases crack-tip constraint.
- The influence of homogenization on residual stress and measured toughness predicted using a micromechanical failure theory shows trends similar to those found experimentally in previous studies.

## Acknowledgments

Funds for the support of this study have been allocated by the NASA-Ames Research Center, Moffett Field, California, under Interchange No. NCC2-5214. The assistance of Owen Nishioka is greatly appreciated.

## References

- [1] T. L. Panontin and M. R. Hill, "The effect of residual stresses on brittle and ductile fracture initiation predicted by micromechanical models," *International Journal of Fracture* 82 (1996) pp. 317-333.
- [2] T. Mura, *Micromechanics of Defects in Solids*, Dordrecht, Netherlands, M. Nijhoff (1987)
- [3] M. R. Hill, Ph.d. Dissertation, Stanford University (1996).
- [4] J. A. Goldak, et al., "Computational Weld Mechanics," *Advanced Joining of Materials* (AGARD CP-398), AGARD (1985) pp. 1-1 - 1-32.
- [5] Y. Ueda, K. Nakacho, and M. Yuan, "Application of FEM to theoretical analysis, measurement and prediction of welding residual stresses," *Transactions of the Japanese Welding Research Institute* 20(1) (1991) pp. 97-107
- [6] M. R. Hill and D. V. Nelson, "The Inherent Strain Method for Residual Stress Determination and Its Application to a Long Welded Joint," *ASME Pressure Vessels and Piping* 318 (1995) pp. 343-352.
- [7] R. Gunnert, "Residual Stresses," *Proceedings of the Special Symposium on the Behavior of Welded Structures, Urbana, IL*, University of Illinois Engineering Experiment Station (1961) pp. 164-201.
- [8] V. Kumar, M. D. German, and C. F. Shih, "An Engineering Approach for Elastic-Plastic Fracture Analysis," EPRI Report NP-1931, Electric Power Research Institute, Palo Alto (1981).
- [9] W. A. Sorem, S. T. Rolfe, and R. H. Dodds, Jr., "The Effects of Crack Depth on Elastic-Plastic CTOD Fracture Toughness," *Welding Research Council Bulletin* 351 (1990) pp. 12-23.
- [10] R. O. Ritchie, W. L. Server, and R. A. Wullarert, "Critical Fracture Stress and Fracture Strain Models for the Prediction of Lower and Upper Shelf Toughness in Nuclear Pressure Vessel Steels," *Metallurgical Transactions* 10A (1979) pp. 1557-1570.
- [11] A. C. Mackenzie, J. W. Hancock, and D. K. Brown, "On the Influence of State of Stress on Ductile Failure Initiation in High Strength Steels," *Engineering Fracture Mechanics* 9 (1977) pp. 167-188.

- [12] N. P. O'Dowd and C. F. Shih, "Family of Crack-Tip Fields Characterized by a Triaxiality Parameter: Part I-Structure of Fields," *Journal of the Mechanics and Physics of Solids* 39 (1991) pp. 989-1015.
- [13] N. P. O'Dowd and C. F. Shih, "Family of Crack-Tip Fields Characterized by a Triaxiality Parameter: Part II-Fracture Applications," *Journal of the Mechanics and Physics of Solids*, 40 (1992) pp. 939-963.
- [14] M. Nevalainen and R. H. Dodds, Jr., "Numerical Investigation of 3-D Constraint Effects on Brittle Fracture in SE(B) and C(T) Specimens," Report UIUC-ENG-95-2001, University of Illinois at Urbana-Champaign (1995).
- [15] P3/PATRAN, *User Manual, Release 1.3*, PDA Engineering, Inc., Los Angeles, CA (1994).
- [16] *ABAQUS/Standard, User's Manual, Version 5.5*, Hibbitt, Karlsson, and Sorenson, Inc., Providence, RI (1995).
- [17] P. W. Bridgman, *Studies in Large Flow and Fracture*, McGraw-Hill, New York (1952).
- [18] G. Glinka and G. Shen, "Universal Features of Weight Functions for Cracks in Mode I," *Engineering Fracture Mechanics* 40 (1991) pp. 1135-1146.
- [19] T. L. Panontin and S. D. Sheppard, "An Experimentally-Verified Finite Element Study of the Stress-Strain Response of Crack Geometries Experiencing Large Scale Yielding," *Fatigue and Fracture Mechanics, 27th Volume, ASTM STP 1296*, Robert S. Piasek, James C. Newman, Jr. and Norman E. Dowling, Eds., American Society for Testing and Materials (1997) pp. 216-242.
- [20] T. L. Panontin, Ph.d. Dissertation, Stanford University (1994).
- [21] E. F. Rybicki and J. R. Shadley, "A Three-dimensional Finite Element Evaluation of a Destructive Experimental Method of Determining Through-thickness Residual Stresses in Girth Welded Pipes," *Journal of Engineering Materials and Technology* 108(2) (1986) pp. 99-106.
- [22] O. L. Towers and M. G. Dawes, "Welding Institute Research on the Fatigue Precracking of Fracture Toughness Specimens," *Elastic-Plastic Fracture Test Methods: The Users' Experience, ASTM STP 856*, E. T. Wessel and F. J. Loss Eds., American Society for Testing and Materials (1985) pp. 23-46.
- [23] R. H. Leggatt and M. S. Kamath, *Residual Stresses in 25mm Thick Weld Metal COD Specimens in the As-welded and Locally Compressed States*, The Welding Institute (1981).